

Video Object Segmentation using Supervoxel-Based Gerrymandering

Brent A. Griffin and Jason J. Corso
 University of Michigan
 Ann Arbor
 {griffb, jjcorso}@umich.edu

Abstract

Pixels operate locally. Superpixels have some potential to collect information across many pixels; supervoxels have more potential by implicitly operating across time. In this paper, we explore this well established notion thoroughly analyzing how supervoxels can be used in place of and in conjunction with other means of aggregating information across space-time. Focusing on the problem of strictly unsupervised video object segmentation, we devise a method called supervoxel gerrymandering that links masks of foregroundness and backgroundness via local and non-local consensus measures. We pose and answer a series of critical questions about the ability of supervoxels to adequately sway local voting; the questions regard type and scale of supervoxels as well as local versus non-local consensus, and the questions are posed in a general way so as to impact the broader knowledge of the use of supervoxels in video understanding. We work with the DAVIS dataset and find that our analysis yields an unsupervised method that outperforms all other known unsupervised methods and even many supervised ones.

1. Introduction

Video understanding remains a focus area in vision. A critical sub-problem, video object segmentation, supports learning object class models [22, 29], scene parsing [17, 32] and action recognition [19, 27, 28], and many video editing applications [4]. Despite its utility, however, due to the diversity of characteristics videos exhibit and the attendant challenges they present to the assumptions of many segmentation frameworks, finding general solutions for video object segmentation remains a largely unsolved problem.

In an attempt to address some of the challenges in video object segmentation, Faktor and Irani [7] relate superpixels in a high-dimensional region space across many frames, thereby mitigating issues arising from foreground objects with inconsistent optical flow or visual saliency properties. However, while superpixels are restricted to individ-



Figure 1: Video Object Segmentation of Parkour video in DAVIS dataset. Characteristics of this video include a moving camera and a dynamic foreground object.

ual frames and *must* be related across videos by a manufactured coordinate space, supervoxels exhibit an inherent benefit of existing across many frames of video. To this end, we introduce a video segmentation framework that, starting from an initial pixel-level estimate of “foregroundness,” builds an internal consensus within the bounds of each supervoxel, and then relates this local consensus across the entire video for a final determination of the foreground segmentation. We conceptualize this approach to swaying the “foregroundness” of a certain pixel akin to gerrymandering in voting.

Our method has two parts. First, to build an initial quantitative estimate of “foregroundness,” we use a combination of motion and visual saliency cues that are weighted using a straightforward statistical measure of “outlierness” [34]. Second, using the initial estimate we build an internal or local consensus in supervoxels that is then relayed across the video amongst a set of nearest neighbors, which forms an additional non-local consensus. Among the many benefits of extending consensus-based segmentation to supervoxels, we find that a three-dimensional feature space forms a reliable non-local consensus, which is a dramatic simplification of the 176-dimensional feature space used to relate superpixels in [7].

However, we find that there are many unanswered questions from the outset of our work. To address this, we design a system of experiments to explicitly answer the following:

- Given the temporal consistency of supervoxels and

their inherent reach through multiple frames compared to superpixels, how useful is the internal or local consensus of supervoxels relative to non-local consensus for video object segmentation?

- Given the availability of multiple methods for generating supervoxels, which methods are the most useful?
- Given the range of hierarchy levels available with supervoxel methods, which levels are the most effective?

In fact, we believe these questions have broader purview in video understanding than strictly the problem in focus here.

We initiate our consideration of supervoxel selection with a comparative study in [36], which found that segmentation by weighted aggregation (SWA) [5, 26] and hierarchical graph-based (GBH) [11] supervoxels perform best and approximately equally-well with respect to spatiotemporal uniformity, object/region boundary detection, region compression, and parsimony. Xu et al. [38] later develop a streaming hierarchical graph-based (SG) segmentation method, which only processes each video frame once and can handle arbitrarily long videos. To answer the supervoxel selection question in the context of this work, we test all three supervoxel methods in our framework and compare their relative performance.

We evaluate the overall efficacy of our supervoxel-based segmentation method using multiple annotated video benchmarks, including the Densely Annotated Video Segmentation (DAVIS) dataset [24] (see Figure 1). DAVIS has been used in propagating annotations forward in the video [21], training convolutional neural networks [12], or both [13, 14]. In this work, we do not consider supervised techniques, whether in the sense of requiring prior annotations, training data, or human-in-the-loop functionality. Although there are indeed many recent developments in supervised methods for many vision problems, we remain interested in exploring the comparatively more transparent and general unsupervised methods; insights to them may later influence supervised methods as well. Despite the simplicity of this approach, we are able to generate more accurate video object segmentations on DAVIS than many supervised techniques [1, 3, 8, 11, 21, 25], and, to the best of the authors’ knowledge, all current results from unsupervised techniques [2, 7, 9, 15, 23, 31, 35]. In our analysis, we thoroughly experiment with all permutations of method configurations to allow us to systematically answer the three questions we posed earlier.

Main contributions Our paper is primarily an analysis paper that asks and answers important questions about the use of supervoxels as a means for consensus in video object segmentation. This analysis, which carefully elucidates when certain supervoxel methods are more appropriate than others, is the main contribution of the paper. However,

a secondary contribution is the actual method, supervoxel gerrymandering, which we developed to support this analysis. Through the analysis our method is able to achieve the highest performance among all known unsupervised methods and higher performance than many supervised methods on the DAVIS video object segmentation benchmark for single objects, which is our focus.

Paper organization The remainder for this paper is organized as follows. Section 2 derives the supervoxel gerrymandering method and saliency outliers for scaling video data. Section 3 defines our motion and visual saliency-based and supervoxel consensus-based implementations of video object segmentation. Section 4 presents our experimental results on the DAVIS and SegTrackv2 datasets with discussion on our findings, and Section 5 provides concluding remarks.

2. Approach

This section derives the foundational concepts of our video segmentation method. While similar components of this methodology appear in other work [7, 30, 34], this unification of concepts results from a fine grain analysis and allows a precise description of the implementation framework introduced in Section 3.

We use supervoxel gerrymandering in conjunction with a baseline method that generates an initial quantitative estimate of “foregroundness” and “backgroundness.” The initial estimate result from a weighted combination of motion and visual saliency cues. The methodology behind the weighted combination is based on the Tukey range test [34] and, as derived in Section 2.2, is generalizable to many classes of video data. From the initial estimate, we use the derivation in Section 2.1 to build a local and non-local supervoxel-based consensus, which improves the overall performance of our video object segmentation framework, which is depicted in Figure 2.

2.1. Supervoxel Gerrymandering

Supervoxel consensus improves an initial video segmentation using supervoxel-level local and non-local consensus voting. Denote an initial mask estimate at each pixel p as $m_{0p} \in \{0, 1\}$, where $m_{0p} = 1$ suggests that p is in a location corresponding to a foreground object. Also we have a set of non-overlapping supervoxels, $S \in \mathcal{S}$, that cover the full set of pixels for a given video; the supervoxels are disjoint. These may be produced by any method and we will make it concrete during the later analysis.

For each supervoxel, the internal or local foreground consensus is defined as

$$f_S := \frac{1}{N_S} \sum_{p \in S} (2m_{0p} - 1), \quad (1)$$

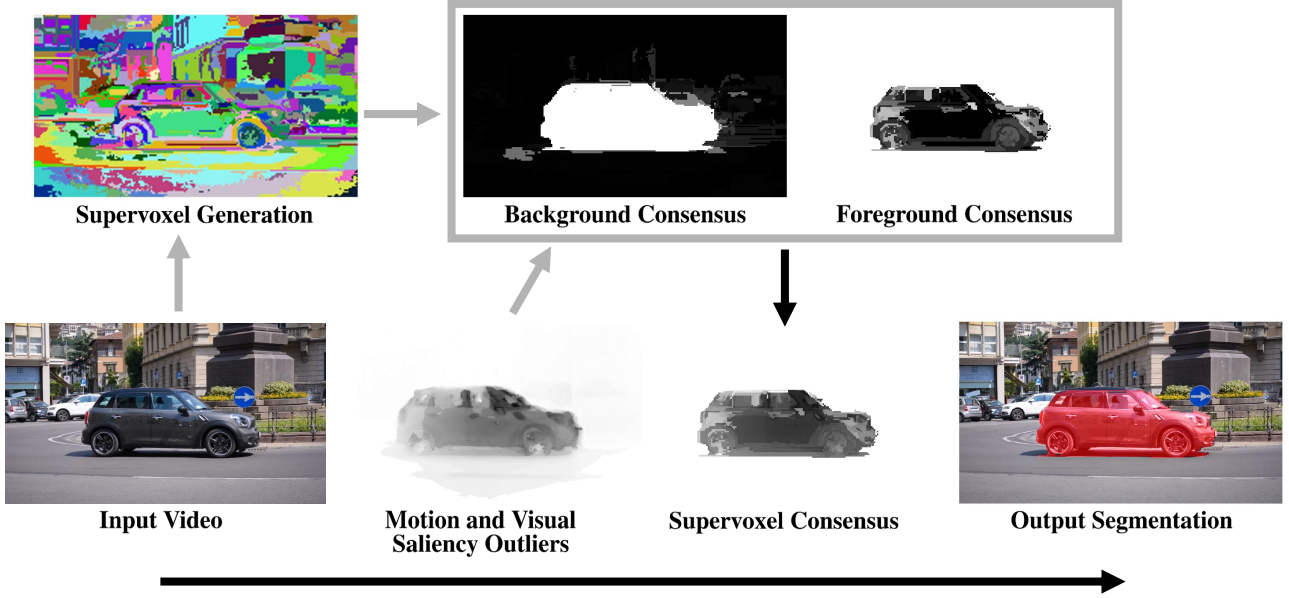


Figure 2: Our segmentation framework uses motion and visual saliency measures as an initial estimate of “foregroundness” (f_{0p} in (11)). Using supervoxels generated from the input video, we refine this initial estimate with a supervoxel-based consensus for both background and foreground elements (f_p in (3)), which determines our output segmentation (m_p in (4)).

where N_S is the number of $p \in S$ and $f_S \in [-1, 1]$. Positive or negative values in (1) correspond to a consensus for S belonging to a foreground object or the background respectively. For each pixel, the supervoxel foreground consensus is defined as

$$f_p^{sc} := w_0 f_{S_0} + \sum_{i=1}^{N_{NL}} w_i f_{S_i}, \quad (2)$$

where f_{S_0} is the local consensus of the supervoxel containing p , N_{NL} is the number of S_0 -nearest-neighbor supervoxels contributing to the non-local consensus, and scalar weights $w_0, w_1, \dots, w_{N_{NL}}$ determine the relative contribution of each supervoxel.

Although an updated foreground mask can be generated directly from (2), we find it more effective in combination with the initial measure used to find m_{0p} . Hence, a final measure is defined as

$$f_p := f_{0p} + f_p^{sc}, \quad (3)$$

where the initial measure f_{0p} improves from f_p^{sc} adding “foregroundness” to pixels with a consistent foreground object consensus and subtracting from pixels with a consistent background consensus as shown in Figure 2. Finally, the updated foreground mask is chosen as

$$m_p := \begin{cases} 1 & \text{if } f_p > 0 \\ 0 & \text{otherwise} \end{cases}. \quad (4)$$

Remarks: (a) For the current work, weights in (2) are chosen such that $\sum_{i=0}^{N_{NL}} w_i = 1$, which, given $f_S \in [-1, 1]$ in (1), implies that $f_p^{sc} \in [-1, 1]$. Correspondingly, f_{0p} is scaled in (3) such that $f_{0p} \in [0, 1]$. (b) The scale and offset to m_{0p} in (1) can be modified to change the relative reward/penalty from a foreground/background consensus.

2.2. Saliency Outliers

Based on the assumption that foreground objects in video exhibit distinct behavior relative to the background, the initial estimate of “foregroundness,” f_{0p} in (3), is found using motion and visual saliency data outliers. Outliers are found in each set of data using a process inspired by Tukey’s range test. Data are divided using a lower and upper outlier thresholds, O_1 and O_3 respectively, that are calculated as

$$O_1 = Q_1 - k(Q_3 - Q_1) \quad (5)$$

$$O_3 = Q_3 + k(Q_3 - Q_1), \quad (6)$$

where Q_1 and Q_3 are the lower and upper quartiles, $Q_3 - Q_1$ is the interquartile range, $k = 1.5$ is a constant that scales the outlier thresholds (for later use in Section 3.1, Q_2 will be considered the median). For a given set of pixel-level data $d_p \in D$, the outliers are defined as

$$O := \{d_p \in D | d_p < O_1 \vee d_p > O_3\}, \quad (7)$$

allowing us to define an ‘‘outlierness’’ scale for weighing each saliency measure as

$$\alpha := \frac{\sum_{d_p \in O} |d_p|}{\sum_{d_p \in D} |d_p|}, \quad (8)$$

where $\alpha \in [0, 1]$ is proportional to the magnitude of outlier data relative to all data.

3. Implementation Framework

This section describes the fully implemented segmentation framework. Section 3.1 details the initial quantitative measure of ‘‘foregroundness’’ and attendant mask. Section 3.2 describes the supervoxel consensus implementation that improves the initial foreground estimate for the final output mask. For the sake of completeness and repeatability, source code is provided at [10].

3.1. Initial Segmentation via Saliency Outliers

This initial estimate of ‘‘foregroundness,’’ f_{0p} , is found using a weighted combination of motion and visual saliency measures. For motion saliency, x and y optical flow components are found using [18]. Using the x and y flow components, the flow magnitude (i.e., $|x^2 + y^2|$) and flow angle (i.e., $\arctan(\frac{y}{x})$) are also calculated. For each flow measure, the outlier thresholds and scales are calculated on a frame-to-frame basis using (5)-(8). The pixel-level measure of motion saliency, d_p^{ms} , is defined for each flow component as

$$d_p^{ms} := \begin{cases} 0 & \text{if } d_p \notin O \vee \alpha_f < 0.5 \\ \alpha_f |d_{fp} - Q_{f2}| & \text{otherwise} \end{cases}, \quad (9)$$

where d_{fp} is a flow component with corresponding frame-to-frame median Q_{f2} , outlier scale α_f , and a 0.5 minimum scale requirement. The intuition behind (9) is simple: whether a foreground object is moving with a fixed camera or vice versa, the foreground object’s deviation from the frame’s median optical flow will generally be salient; the absolute value enables a positive ‘‘foregroundness’’ contribution regardless of a flow component’s sign; and the minimum scale requirement will remove the influence of less reliable flow components.

For video segmentation, we have found that in most cases visual saliency is less reliable than optical flow. However, the product of visual saliency and optical flow is beneficial for videos with dynamic background elements. Thus, the pixel-level measure of visual saliency, d_p^{vs} , is defined as

$$d_p^{vs} := d_{vp}^k \sum_{i=1}^4 \max(\alpha_{f_i}, 0.5) |d_{f_{ip}} - Q_{f_{i2}}|, \quad (10)$$

where $d_{vp} \in [0, 1]$ is a pixel-level visual saliency-based scale (found using [20]), k is an exponential scale that adjusts the relative sharpness of $d_{vp}^k \in [0, 1]$, $d_{f_{ip}}$ is the i th flow component with corresponding median $Q_{f_{i2}}$ and outlier scale α_{f_i} , and the minimum applied scale of 0.5 ensures that visual saliency measures are available even if $\alpha_{f_i} = 0 \forall i$. Three visual saliency measures are used altogether, with $k = \{1, \frac{1}{2}, \frac{1}{3}\}$.

Finally, the initial foreground measure, f_{0p} , is defined as

$$f_{0p} := \sum_{i=1}^{N_D} d_p^i, \quad (11)$$

where d_p^i is the i th component of $N_D = 7$ saliency measures (four from (9) and three from (10)). Using (11), the initial foreground mask, m_{0p} , is found using (4), but with the following threshold: $f_{0p} > \beta_p \delta_p$, where $\beta_p \in \mathbb{R}$ is the sum of the mean and standard deviation of f_{0p} in the current frame and δ_p is a previous-mask threshold scale defined as

$$\delta_p := \begin{cases} \frac{1}{2} & \text{if } m_{0p, k-1} = 1 \\ 1 & \text{otherwise} \end{cases}, \quad (12)$$

where $m_{0p, k-1}$ represents m_{0p} from the previous frame. In simple words, if f_{0p} is greater than the pixel-level mean and standard deviation of ‘‘foregroundness’’ over the current frame, p is considered a foreground object location. In addition, from (12), wherever p corresponds to a mask position in the previous frame, a half-threshold discount is applied, which generally encourages frame-to-frame segmentation continuity and gradually increasing accuracy of the initial mask. Finally, the initial mask assumes a single foreground object hypothesis. Accordingly, the mask is restricted within each frame to contain a single continuous segment exhibiting the greatest combined values of f_{0p} .

Remark: In the remainder of the paper, the initial foreground mask will be referred to as MVSO (motion and visual saliency outliers).

3.2. Final Segmentation via Supervoxel Consensus

Given the initial foreground estimation from Section 3.1, we now describe our implementation of supervoxel consensus for segmentation. First, we determine the relative consensus weight of each supervoxel used in (2). The local consensus weight, w_0 , changes based on the overall consensus configuration implemented. If implementing only local consensus, $w_0 = 1$ and all of the non-local weights are scaled to zero. If implementing only non-local consensus, $w_0 = 0$ and all non-local weights are uniformly scaled *s.t.* $\sum_{i=1}^{N_{NL}} w_i = 1$. Finally, if implementing both local and non-local consensus, $w_0 = \frac{1}{3}$ and non-local weights are uniformly scaled *s.t.* $\sum_{i=1}^{N_{NL}} w_i = \frac{2}{3}$.

In [7], non-local consensus weights are based on nearest neighbor regions for superpixels that use a 176-dimensional space, which consists of RGB and LAB histograms, HOG descriptors, and relative spatial coordinates. In the current work, non-local weights are based on supervoxel regions that only use a 3 dimensional space, which consists of the mean LAB color of each supervoxel. Specifically, the nominal non-local consensus weights $w_1, \dots, w_{N_{NL}}$ in (2) are chosen as

$$w_i = \frac{1}{R(S_0, S_i)^2}, \quad (13)$$

where $R \in \mathbb{R}$ calculates the city-block distance between the mean-LAB region space of local supervoxel S_0 and the i th nearest neighbor S_i . Because R is squared, the influence of supervoxels outside of the primary “clique” drops off quickly. Furthermore, the LAB region space is normalized for the consensus weight calculation in (13) such that the minimum and maximum video-wide LAB-pixel values correspond to 0 and 1 respectively. This normalization ensures that all three region space dimensions are meaningful, even if their original differences are minor.

Selecting the number of nearest neighbors used for non-local consensus is chosen within the context of the changing number of supervoxels between each video and supervoxel hierarchy. Specifically, N_{NL} in (2) is chosen as $N_{NL} = \frac{1}{N_S}$, where N_S is the total number of supervoxels in the video, $S \in \mathcal{S}$. Scaling the number of nearest neighbors in this manner keeps a relatively consistent ratio of consensus to non-consensus neighbors for varying sizes of videos and supervoxels.

Given the full definition of the implementation consensus terms, f_p^{sc} is calculated using (2) and is combined with f_{0p} from Section 3.1 for the final measure of “foregroundness,” f_p in (3). Using (4), values of $f_p > 0$ determine the locations of the foreground object proposal, m_p . As a final processing step, m_p is restricted within each frame to contain at most two continuous segments exhibiting the greatest combined values of f_p . In this sense, the final foreground segmentation of our framework roughly approximates a single object hypothesis that accounts for limited instances of occlusions.

4. Results

We evaluate our approach on two datasets: the Densely Annotated Video Segmentation (DAVIS) [24] and the Georgia Tech Segmentation and Tracking Dataset (SegTrackv2) [16, 33]. The DAVIS dataset includes videos from 50 diverse scenarios that collectively test the assumptions of many segmentation frameworks. Furthermore, all of the DAVIS dataset’s ground truth annotations match the single object hypothesis. The SegTrackv2 dataset has fewer

videos than DAVIS, and only a subset match the single object hypothesis. However, SegTrackv2 provides an additional challenge by using videos with different resolutions, which span from 76,800 to 230,400 pixels per frame.

Three different, accepted, measures are used to evaluate the performance of our video foreground object segmentation: region similarity \mathcal{J} , contour accuracy \mathcal{F} , and temporal (in-)stability \mathcal{T} , which are all calculated using the definitions provided in [24]. Region similarity (also known as the intersect over union or Jaccard index [6]) provides a straightforward and scale-invariant evaluation of the number of mislabeled foreground pixels with respect to a ground truth annotation. Given a foreground mask M and ground truth annotation G , $\mathcal{J} = \frac{M \cap G}{M \cup G}$. Contour accuracy evaluates the boundary of a segmentation by measuring differences between the closed set of contours for M and G . Finally, temporal stability is a measure based on the consistency of a mask between frames. While temporal stability is important for some applications, such as video editing, it is shown to be generally uncorrelated with region similarity and contour accuracy in [24].

To test the efficacy of our segmentation approach and establish best practices for implementation, we evaluate the relative changes in performance for all permutations of the following configuration options:

- Supervoxel methods: segmentation by weighted aggregation (SWA), hierarchical graph-based segmentation (GBH), and streaming hierarchical graph-based segmentation (SG).
- Supervoxel hierarchy levels: 5-12 for SWA and 0-20 for GBH and SG.
- Consensus methods: local consensus, non-local consensus, and both.

Following this evaluation in Section 4.1, Section 4.2 provides insights into the questions we posed at the beginning of our study.

Remarks: (a) For simplicity, the SWA, GBH, and SG supervoxels are generated using the standard settings provided in the supervoxel library LIBSVX [37]. (b) To improve computation time, supervoxels are processed on a scaled-down resolution for both data sets and scaled back for segmentation. The reduction scale is 1:4 for the DAVIS dataset and 1:2 for SegTrackv2, which uses lower resolution images than DAVIS.

4.1. Dataset Evaluation

DAVIS Here, we present the results of our evaluation experiments using the DAVIS dataset. Best results for each type of configuration are provided in Table 1. To help explain the naming convention, SWA⁰⁶ uses SWA hierarchy

Configuration	Configuration ID									
	MVSO	SWA ⁰⁶	SWA _L ⁰⁸	SWA _{NL} ⁰⁵	GBH ⁰⁰	GBH _L ⁰²	GBH _{NL} ⁰⁰	SG ⁰¹	SG _L ⁰⁰	SG _{NL} ⁰⁰
Supervoxel Method	None	SWA	SWA	SWA	GBH	GBH	GBH	SG	SG	SG
Hierarchy Level	N/A	6	8	5	0	2	0	1	0	0
Local Consensus	N/A	Yes	Yes	No	Yes	Yes	No	Yes	Yes	No
Non-Local Consensus	N/A	Yes	No	Yes	Yes	No	Yes	Yes	No	Yes
Measure	DAVIS Results									
Rank	6th	1st	4th	5th	3rd	2nd	7th	9th	8th	10th
\mathcal{J} Mean \uparrow	0.586	0.676	0.647	0.616	0.648	0.653	0.544	0.495	0.537	0.282
\mathcal{F} Mean \uparrow	0.475	0.639	0.615	0.592	0.61	0.612	0.526	0.488	0.51	0.326
\mathcal{T} Mean \downarrow	0.307	0.310	0.31	0.431	0.33	0.318	0.522	0.425	0.364	0.78
Supervoxel Volume	N/A	3617	24651	1342	9745	32988	9745	292317	155447	155447

Table 1: Results for each combination of supervoxel and consensus method on the DAVIS dataset. Result measures consist of region similarity (\mathcal{J}), contour accuracy (\mathcal{F}), and temporal (in-)stability (\mathcal{T}). For rows with an upward pointing arrow higher numbers are better (e.g., \mathcal{J} mean), and vice versa for rows with downward pointing arrows. Rank is based on \mathcal{J} . Supervoxel volume is calculated as an average over the entire DAVIS dataset.

DAVIS Results for State-of-the-Art Unsupervised Methods													
Measure	Current Results						[7]	[23]	[15]	[2]	[31]	[9]	[35]
	SWA ⁰⁶	GBH _L ⁰²	GBH ⁰⁰	SWA _L ⁰⁸	SWA _{NL} ⁰⁵	MVSO	NLC	FST	KEY	MSG	CVOS	TRC	SAL
\mathcal{J} Rank	1st	2nd	3rd	4th	6th	7th	5th	8th	9th	10th	11th	12th	13th
\mathcal{F} Rank	1st	3rd	4th	2nd	6th	12th	5th	7th	9th	8th	10th	11th	13th
\mathcal{T} Rank	6-7th	8th	10th	6-7th	12th	5th	11th	4th	1st	3rd	2nd	9th	13th
Mean \uparrow	0.676	0.653	0.648	0.647	0.616	0.586	0.641	0.575	0.569	0.543	0.514	0.501	0.426
\mathcal{J} Recall \uparrow	0.847	0.822	0.822	0.823	0.756	0.759	0.731	0.652	0.671	0.636	0.581	0.560	0.386
Decay \downarrow	0.040	0.024	0.036	0.033	0.032	0.023	0.086	0.044	0.075	0.028	0.127	0.050	0.084
Mean \uparrow	0.639	0.612	0.610	0.615	0.592	0.475	0.593	0.536	0.503	0.525	0.490	0.478	0.383
\mathcal{F} Recall \uparrow	0.785	0.755	0.768	0.755	0.708	0.488	0.658	0.579	0.534	0.613	0.578	0.519	0.264
Decay \downarrow	0.057	0.040	0.060	0.046	0.054	0.014	0.086	0.065	0.079	0.057	0.138	0.066	0.072
\mathcal{T} Mean \downarrow	0.310	0.318	0.330	0.310	0.431	0.307	0.356	0.276	0.190	0.250	0.243	0.327	0.600

Table 2: Comparison of our segmentation method with other state-of-the-art unsupervised methods on the DAVIS dataset. Bold text indicates the best performance for a specific measure. Multiple combinations of supervoxel and consensus method achieve state-of-the-art results. The current work is only outperformed in temporal (in-)stability (\mathcal{T}). Object recall measures the fraction of sequences scoring higher than 0.5, and decay quantifies the performance loss (or gain) over time [24]. MVSO exhibits the best decay performance for region similarity and contour accuracy, which is likely the result of the previous-mask threshold discount (12) implemented on MVSO, which encourages gradually increasing accuracy of the initial mask.

level 6 and represents the best results for any SWA configuration using both local and non-local consensus, while GBH_L⁰² uses GBH hierarchy level 2 and represents the best results for any GBH configuration using only local consensus.

The best result for region similarity (\mathcal{J}) and contour accuracy (\mathcal{F}) both come from SWA⁰⁶, which uses both forms of consensus and the second lowest hierarchy available to SWA. GBH_L⁰² has the second best \mathcal{J} and third best \mathcal{F} and uses only local consensus on the third lowest hierarchy available to GBH. GBH⁰⁰ has the third best \mathcal{J} , and SWA_L⁰⁸ has the second best \mathcal{F} . The best result using only non-local consensus is SWA_{NL}⁰⁵, which achieves a middle result of the

5th best \mathcal{J} and uses the lowest SWA hierarchy. The significance of this hierarchy is that it has the smallest supervoxel volume and largest number of supervoxels to form a non-local consensus. Overall, SG configurations have the worst results and largest supervoxels. The SG non-local consensus configuration, SG_{NL}⁰⁰, has the worst performance in all categories. The initial mask configuration, MVSO from Section 3.1, has a better \mathcal{J} result than all SG configurations and GBH_{NL}⁰⁰, but the second worst contour.

The region similarity results for all configurations are shown in Figure 3. In all cases, performance eventually decreases with increasing hierarchy level and supervoxel size, although the local consensus configuration groups SWA_L

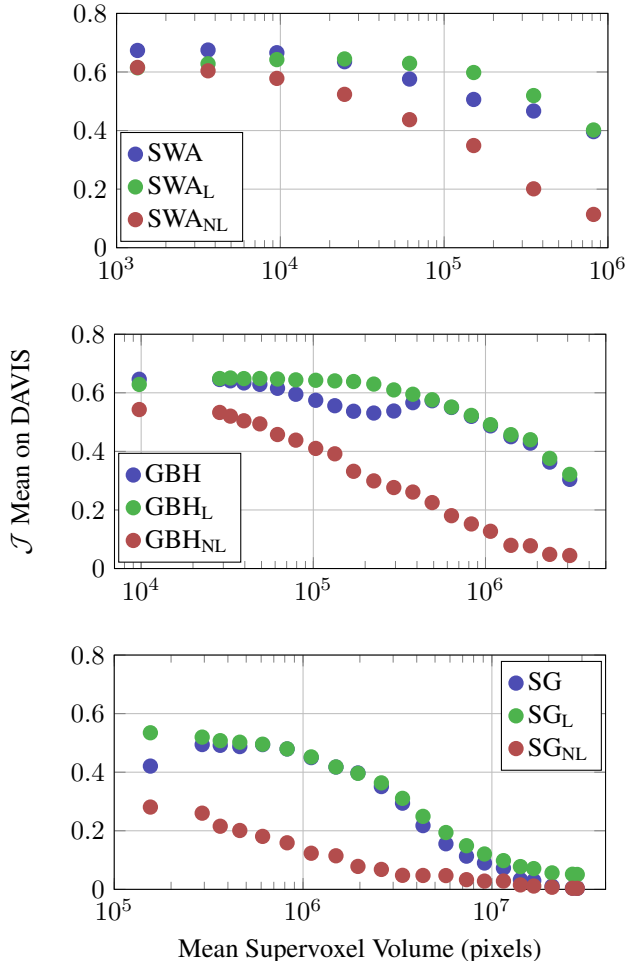


Figure 3: \mathcal{J} mean on the DAVIS dataset vs. mean supervoxel volume for SWA hierarchy levels 5-12 (top), GBH 0-20 (middle), and SG 0-20 (bottom). Mean supervoxel volumes increase with hierarchy level.

and GBH_L hold out against this trend longer than their counterpart configurations. At the highest hierarchy levels, SWA and GBH configurations, which use both local and non-local consensus, converge on SWA_L and GBH_L as the number of non-local consensus neighbors decreases with the number of supervoxels (recall from Section 3.2 that $N_{\text{NL}} = \frac{1}{N_S}$).

Finally, the current work is compared with the current state-of-the-art unsupervised segmentation methods in Table 2 and the current state-of-the-art supervised segmentation methods in Table 3, with more discussion provided in Section 4.2.

SegTrackv2 Table 4 shows the results of an additional evaluation using the SegTrackv2 dataset. The videos included in our evaluation are those that use a single hypothe-

sis annotation, which is consistent with the DAVIS dataset. However, SegTrackv2 also presents the challenge of using videos with different video resolutions, spanning from 76,800 to 230,400 pixels per frame. This is challenging because a configuration with a constant supervoxel hierarchy level will have a dramatically different number of supervoxels from one video to the next. To remedy this limitation, we introduce an additional set of configurations, labeled with an “ALL,” that can switch supervoxel hierarchy levels for each video, which is shown to provide a slight increase in performance. Compared with the DAVIS dataset, GBH and SG configuration exhibit an increase in performance, and SWA configurations and MVSO exhibit a decrease in performance. It is also worth noting that an increase in performance from MVSO would likely improve the results of all other configurations since it forms the initial basis for supervoxel consensus.

4.2. Discussion

Local vs. Non-Local Consensus From Figure 3, it is evident that our non-local consensus framework is heavily reliant on using a low-level hierarchy, and quickly loses performance as supervoxel size increases and the attendant number of available neighbors for consensus decreases. The local consensus framework, on the other hand, exhibits a greater robustness to increasing hierarchy levels, which makes intuitive sense since larger supervoxels will be able to draw on more internal pixels throughout a video for a better informed consensus. Multiple local consensus configurations achieve the best results of the current work on the SegTrackv2 dataset (see Table 4), and also exhibit some of the best results on the DAVIS dataset. Still, it is worth noting that the SWA^{06} configuration, which uses both local and non-local consensus, achieves the best results on the DAVIS dataset, which implies that there are merits to using both forms of consensus when using a hierarchy level where both are independently effective (see Figure 3 top).

All consensus-based methods exhibit a poorer temporal stability (\mathcal{T}) relative to the other methods presented in Table 2. This likely occurs from discrete consensus-based changes in the segmentation mask that can occur from frame to frame. However, methods using local supervoxel consensus appear to be less effected by this phenomena than the non-local consensus-based $\text{SWA}_{\text{NL}}^{05}$ or non-local superpixel-consensus based NLC.

Choice of Supervoxel Method The SWA configuration SWA^{06} exhibits the best performance on the DAVIS dataset (see Table 1). However, GBH configurations consist of the second and third best performances, and the two best performances of the current work on the SegTrackv2 dataset, which has a variable resolution between videos. Thus, of the three methods, GBH appears to be the most robust

Comparison of DAVIS Results with Supervised Methods										
Measure	[13]	[14]	[12]	Current Results	[21]	[25]	[8]	[11]	[1]	[3]
	VPND	MSKT	FUSG	SWA ⁰⁶	BVS _Q	FCP	JMP	HVS	SEA	TSP
\mathcal{J} Mean	0.750	0.748	0.715	0.676	0.67	0.631	0.607	0.596	0.556	0.358

Table 3: Comparison of our unsupervised segmentation method with supervised methods on the DAVIS dataset.

SegTrackv2 Results												
Video	Unsupervised								Supervised			
	Current Results								[7]	[15]	[23]	[12]
\mathcal{J} Mean	GBH _L ^{ALL}	GBH _L ⁰⁹	SWA ^{ALL}	SG _L ^{ALL}	SWA ⁰⁵	SG _L ⁰¹	MVSO	NLC	KEY	FST	FUSG	HVS
Rank	2nd	3rd	5th	6th	7th/8th	9th	12th	1st	4th	11th	7th/8th	10th
Birdfall	0.62	0.62	0.54	0.50	0.54	0.49	0.23	0.74	0.49	0.18	0.38	0.57
Frog	0.78	0.74	0.50	0.47	0.50	0.44	0.61	0.83	0.00	0.54	0.57	0.67
Girl	0.69	0.67	0.70	0.64	0.70	0.62	0.65	0.91	0.88	0.55	0.67	0.32
Monkey	0.58	0.52	0.57	0.60	0.44	0.49	0.34	0.71	0.79	0.65	0.80	0.62
Parachute	0.88	0.88	0.88	0.86	0.86	0.85	0.67	0.94	0.96	0.76	0.52	0.69
Soldier	0.56	0.49	0.53	0.63	0.53	0.58	0.49	0.83	0.67	0.40	0.70	0.67
Worm	0.77	0.75	0.58	0.58	0.58	0.58	0.52	0.81	0.84	0.73	0.51	0.35
All	0.70	0.67	0.62	0.61	0.59	0.58	0.50	0.82	0.66	0.54	0.59	0.56

Table 4: Comparison of our segmentation method with other state-of-the-art methods on the SegTrackv2 dataset. Bold text indicates the best performance for each video. Methods labeled with an “ALL” can switch supervoxel hierarchies for each video, which have different resolutions on the SegTrackv2 dataset. Selected videos consist of a single foreground object hypothesis. Results for other methods come from comparative studies in [7, 12].

framework with respect to video scale and variability.

SG configurations have the worst performance of the current methods on the DAVIS dataset, however, they exhibit an improvement on the SegTrackv2 dataset and operate in a streaming format, which works well for long videos and is necessary for any eventual real-time application. In the end, we propose that SG should only be considered if streaming or better runtime performance on longer videos is necessary, while both GBH and SWA methods warrant further investigation for the general video segmentation problem.

Choice of Supervoxel Hierarchy Level In Figure 3, the overall trend is clear that performance eventually drops when using the highest hierarchy levels. This intuitive makes sense because larger supervoxels in high hierarchy levels are more likely to have segmented over a meaningful foreground object boundary. Low hierarchy levels also enable non-local consensus forming with larger groups of relevant supervoxels. However, it is not necessarily the rule that the lowest level hierarchy exhibits the best performance, especially for local consensus methods that rely on individual supervoxel volumes to form a meaningful internal consensus. Additionally, it is shown in Table 4 that solutions that are able to draw on multiple hierarchy levels (the “All” configurations) exhibit a meaningful improvement in performance. In general, it seems like the best segmenta-

tion performance occurs in the lower level regions, however a range of hierarchy levels should be employed to ensure the best segmentation performance.

5. Conclusion

At the outset of our work, we proposed to answer several questions arising from the use of supervoxels for consensus-based video object segmentation. First, we find that local consensus is imperative for the video object segmentation problem and is more useful than non-local consensus. Second, hierarchical graph-based segmentation (GBH) supervoxel methods are the most reliable. Finally, the lowest hierarchy levels are most effective for non-local consensus, whereas low- and mid-hierarchy levels are effective for local consensus. In the context of video object segmentation, the highest hierarchy levels are not effective.

We find that this study is but one of many studies that have potential to shed light on the capability that supervoxels play in video understanding. Furthermore, given the performance of the current work on accepted benchmarks, we postulate that such studies are worthwhile for the video object segmentation problem. Given that the current work is restricted to a single object hypothesis, we are currently working on extending this analysis to a multiple object hypothesis.

Source code for the current work is provided at [10].

Acknowledgements

This work was partially supported by the DARPA MediFor program under contract FA8750-16-C-0168.

References

- [1] S. Avinash Ramakanth and R. Venkatesh Babu. Seamseg: Video object segmentation using patch seams. In *Proceedings of the IEEE Conference on Computer Vision and Pattern Recognition*, pages 376–383, 2014. 2, 8
- [2] T. Brox and J. Malik. Object segmentation by long term analysis of point trajectories. In *European conference on computer vision*, pages 282–295. Springer, 2010. 2, 6
- [3] J. Chang, D. Wei, and J. W. Fisher. A video representation using temporal superpixels. In *Proceedings of the IEEE Conference on Computer Vision and Pattern Recognition*, pages 2051–2058, 2013. 2, 8
- [4] D.-J. Chen, H.-T. Chen, and L.-W. Chang. Video object cosegmentation. In *ACM International Conference on Multimedia*, 2012. 1
- [5] J. J. Corso, E. Sharon, S. Dube, S. El-Saden, U. Sinha, and A. Yuille. Efficient multilevel brain tumor segmentation with integrated bayesian model classification. *IEEE transactions on medical imaging*, 27(5):629–640, 2008. 2
- [6] M. Everingham, L. Van Gool, C. K. Williams, J. Winn, and A. Zisserman. The pascal visual object classes (voc) challenge. *International journal of computer vision*, 88(2):303–338, 2010. 5
- [7] A. Faktor and M. Irani. Video segmentation by non-local consensus voting. In *BMVC*, volume 2, page 8, 2014. 1, 2, 5, 6, 8
- [8] Q. Fan, F. Zhong, D. Lischinski, D. Cohen-Or, and B. Chen. Jumpcut: non-successive mask transfer and interpolation for video cutout. *ACM Trans. Graph.*, 34(6):195, 2015. 2, 8
- [9] K. Fragkiadaki, G. Zhang, and J. Shi. Video segmentation by tracing discontinuities in a trajectory embedding. In *Computer Vision and Pattern Recognition (CVPR), 2012 IEEE Conference on*, pages 1846–1853. IEEE, 2012. 2, 6
- [10] B. Griffin and J. Corso. Video object segmentation source code for the current work: <https://github.com/griffbr/supervoxel-gerrymandering>, 2017. 4, 8
- [11] M. Grundmann, V. Kwatra, M. Han, and I. Essa. Efficient hierarchical graph-based video segmentation. In *2010 IEEE Computer Society Conference on Computer Vision and Pattern Recognition*, pages 2141–2148, June 2010. 2, 8
- [12] S. D. Jain, B. Xiong, and K. Grauman. Fusionseg: Learning to combine motion and appearance for fully automatic segmentation of generic objects in videos. *arXiv preprint arXiv:1701.05384*, 2017. 2, 8
- [13] V. Jampani, R. Gadde, and P. V. Gehler. Video propagation networks. *arXiv preprint arXiv:1612.05478*, 2016. 2, 8
- [14] A. Khoreva, F. Perazzi, R. Benenson, B. Schiele, and A. Sorkine-Hornung. Learning video object segmentation from static images. *arXiv preprint arXiv:1612.02646*, 2016. 2, 8
- [15] Y. J. Lee, J. Kim, and K. Grauman. Key-segments for video object segmentation. In *Computer Vision (ICCV), 2011 IEEE International Conference on*, pages 1995–2002. IEEE, 2011. 2, 6, 8
- [16] F. Li, T. Kim, A. Humayun, D. Tsai, and J. M. Rehg. Video segmentation by tracking many figure-ground segments. In *The IEEE International Conference on Computer Vision (ICCV)*, December 2013. 5
- [17] B. Liu and X. He. Multiclass semantic video segmentation with object-level active inference. In *IEEE Conference on Computer Vision and Pattern Recognition*, 2015. 1
- [18] C. Liu. *Beyond pixels: exploring new representations and applications for motion analysis*. PhD thesis, Citeseer, 2009. 4
- [19] J. Lu, R. Xu, and J. J. Corso. Human action segmentation with hierarchical supervoxel consistency. In *IEEE Conference on Computer Vision and Pattern Recognition*, 2015. 1
- [20] R. Margolin, A. Tal, and L. Zelnik-Manor. What makes a patch distinct? In *Proceedings of the IEEE Conference on Computer Vision and Pattern Recognition*, pages 1139–1146, 2013. 4
- [21] N. Märki, F. Perazzi, O. Wang, and A. Sorkine-Hornung. Bilateral space video segmentation. In *Proceedings of the IEEE Conference on Computer Vision and Pattern Recognition*, pages 743–751, 2016. 2, 8
- [22] D. Oneata, J. Revaud, J. Verbeek, and C. Schmid. Spatio-temporal object detection proposals. In *European Conference on Computer Vision*, 2014. 1
- [23] A. Papazoglou and V. Ferrari. Fast object segmentation in unconstrained video. In *Proceedings of the IEEE International Conference on Computer Vision*, pages 1777–1784, 2013. 2, 6, 8
- [24] F. Perazzi, J. Pont-Tuset, B. McWilliams, L. Van Gool, M. Gross, and A. Sorkine-Hornung. A benchmark dataset and evaluation methodology for video object segmentation. In *Proceedings of the IEEE Conference on Computer Vision and Pattern Recognition*, pages 724–732, 2016. 2, 5, 6
- [25] F. Perazzi, O. Wang, M. Gross, and A. Sorkine-Hornung. Fully connected object proposals for video segmentation. In *Proceedings of the IEEE International Conference on Computer Vision*, pages 3227–3234, 2015. 2, 8
- [26] E. Sharon, M. Galun, D. Sharon, R. Basri, and A. Brandt. Hierarchy and adaptivity in segmenting visual scenes. *Nature*, 442(7104):810–813, 2006. 2
- [27] K. Soomro, H. Idrees, and M. Shah. Action localization in videos through context walk. In *IEEE International Conference on Computer Vision*, 2015. 1
- [28] K. Soomro, H. Idrees, and M. Shah. Predicting the where and what of actors and actions through online action localization. In *IEEE Conference on Computer Vision and Pattern Recognition*, 2016. 1
- [29] K. Tang, R. Sukthankar, J. Yagnik, and L. Fei-Fei. Discriminative segment annotation in weakly labeled video. In *IEEE Conference on Computer Vision and Pattern Recognition*, 2013. 1
- [30] E. H. Taralova, F. De la Torre, and M. Hebert. Motion words for videos. In *European Conference on Computer Vision*, pages 725–740. Springer, 2014. 2

- [31] B. Taylor, V. Karasev, and S. Soatto. Causal video object segmentation from persistence of occlusions. In *Proceedings of the IEEE Conference on Computer Vision and Pattern Recognition*, pages 4268–4276, 2015. [2](#), [6](#)
- [32] J. Tighe and S. Lazebnik. Superparsing: scalable nonparametric image parsing with superpixels. *International Journal of Computer Vision*, 2012. [1](#)
- [33] D. Tsai, M. Flagg, A. Nakazawa, and J. M. Rehg. Motion coherent tracking using multi-label mrf optimization. *International journal of computer vision*, 100(2):190–202, 2012. [5](#)
- [34] J. W. Tukey. Exploratory data analysis. 1977. [1](#), [2](#)
- [35] W. Wang, J. Shen, and F. Porikli. Saliency-aware geodesic video object segmentation. In *Proceedings of the IEEE Conference on Computer Vision and Pattern Recognition*, pages 3395–3402, 2015. [2](#), [6](#)
- [36] C. Xu and J. J. Corso. Evaluation of super-voxel methods for early video processing. In *Computer Vision and Pattern Recognition (CVPR), 2012 IEEE Conference on*, pages 1202–1209. IEEE, 2012. [2](#)
- [37] C. Xu and J. J. Corso. Libsvx: A supervoxel library and benchmark for early video processing. *International Journal of Computer Vision*, 119(3):272–290, 2016. [5](#)
- [38] C. Xu, C. Xiong, and J. J. Corso. Streaming hierarchical video segmentation. In *European Conference on Computer Vision*, pages 626–639. Springer, 2012. [2](#)